© 2017 Jinhong Kim

RECONFIGURABLE, TWO-DIMENSIONAL PLASMA
PHOTONIC CRYSTALS

BY

JINHONG KIM

THESIS

Submitted in partial fulfillment of the requirements
for the degree of Master of Science in Electrical and Computer Engineering
in the Graduate College of the
University of Illinois at Urbana-Champaign, 2017

Urbana, Illinois

Adviser:

Professor J. Gary Eden

ABSTRACT

Photonic crystals, composed of arrays of microplasmas, affect the propagation of electromagnetic waves and can act as reconfigurable filters in the GHz-THz spectral regions. Plasma photonic crystals are reconfigurable at electronic speeds. In addition, they rapidly alter the transmission characteristics, relative to photonic crystals fabricated in a solid. This thesis describes the characteristics and performance of photonic crystals based on arrays of microplasma jets.

To my family

ACKNOWLEDGMENTS

My utmost gratitude goes to my adviser, Professor J. Gary Eden, for his invaluable guidance and consistent support of my research. I would also like to express my gratitude to Professor Sung-Jin Park, who provided insightful comments and support in overcoming numerous obstacles I faced through my research. Besides my advisors, I am thankful for all members of the Laboratory for Optical Physics and Engineering for their feedback, cooperation and of course friendship. Last but not the least, I would like to thank my family: my parents and my sisters for their unfailing spiritual supporting and continuous encouragement throughout my years of study. This accomplishment would not have been possible without them. Thank you.

TABLE OF CONTENTS

CHAPTER 1

INTRODUCTION

Photonic crystals are structures with periodic arrangement of dielectric materials, which provide the ability to reflect a specific range of wavelengths. The structure can control the flow of light and electromagnetic waves. Multiple reflections from each surface that is separated by a certain distance prevent an electromagnetic wave from propagating through the crystal [1]. Several types of photonic crystals have drawn much attention from researchers in recent years. However, there have been limitations to expanding the studies. For example, it is difficult to control the band gap of metal semiconductor photonic crystals due to their lattice limitations. For the normal photonic crystals composed of solid materials, the frequency range of the electromagnetic waves for control is fixed once the periodic structure is fabricated. The parameters determining the position and the width of the photonic band gaps, such as the dielectric constant, the lattice constant, and the symmetry of the structure, are difficult to change.

Alternately, plasma is a good candidate to replace the conventional solid dielectric materials in photonic crystals. One of the most attractive properties of plasma photonic crystals is the tunable photonic band gap that can be controlled by plasma parameters [1]. Plasma parameters can be varied freely by adjusting external parameters, leading to a large and tunable range of the electromagnetic wave frequency. Due to these special properties of plasma photonic crystals, technological applications are promising and include plasma antennas, narrow band filters, and plasma lenses.

In this thesis, microplasma devices with a lattice constant of 1 mm will be utilized to reconfigure the photonic crystal in the GHz-THz region. The two greatest advantages of

microplasma-based photonic crystals are the ability to control the refractive index and alter their characteristics at electronic speeds. The properties of 2-D plasma photonic crystals and their fundamental characteristics will be discussed in the next chapters.

CHAPTER 2

LOW TEMPERATURE PLASMA FUNDAMENTALS

2.1. Microplasma and Paschen's Curve

Plasma is generally referred to as the fourth fundamental state of matter. It is collection of ions, free electrons, and neutral molecules. In most plasmas, ions and electrons are present in equal numbers, making them electrically quasi-neutral (electron density $n_e \cong$ ion density n_i) with less than 1% fractional ionization. Microplasma is described as a type of plasma that is generated in a microscale discharge gap. As shown in Figure 1, Paschen's curve indicates the minimum breakdown voltage of a discharge for a noble gas as a function of pressure (p) and the distance between two electrodes (d), which is a reliable guide to predict the parameters of discharges [2]. Compared with conventional plasmas, microplasma can be operated at higher pressure. As shown in Figure 1, low pressure is essential to generate conventional plasma, such as for a fluorescent lamp, due to large-scale d ($d > 10$ mm) in order to minimize the breakdown voltage; however, microplasma can be generated in both low pressure and atmospheric pressure (780 Torr) because of microscale d [3].

Significant characteristics of microplasma include its non-equilibrium state, in that the electron, ion, and gas temperatures are not the same [2, 4]. The gas temperature is much lower than the electron temperature because the average energy exchange in collision of ions and electrons increases when plasma is confined in a small gap. Thus, microplasma in microscale discharge gap at constant pressure leads to an increase of electron temperature. Typical values for the electron temperature is $1 - 5$ eV and ion temperature is typically 0.1 eV, while gas temperature for noble gas (<500 K) is generally as low as room temperature [3, 5, 6].
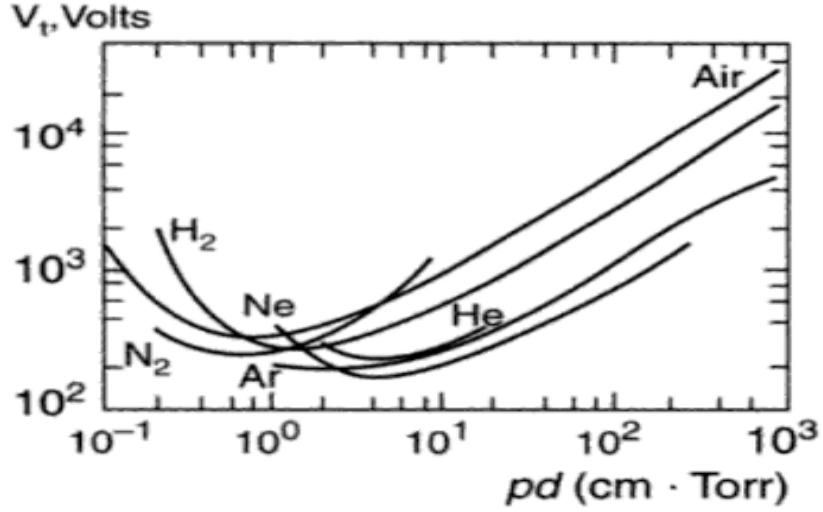
Figure 1. Paschen's curve breakdown voltage as a function of pressure and gap between electrodes [2].

2.2. Debye Length

In plasma physics, the concepts of Debye length and sheath region are essential to plasma studies. The Debye length, λ_D, is the minimum distance over which electric charges can be screened, retaining the quasi-neutrality of the bulk plasma. The Debye length equation can be derived using Poisson's equation, which describes the potential field caused by charge density distribution, and is given by

$$\nabla^2 \Phi = -\frac{\rho}{\varepsilon_0} \tag{2.1}$$

where ρ is the charge density (C/cm^3), ε_0 is the vacuum permittivity (F/m), and Φ is the electric potential (V). In order to determine λ_D, simply assume that the immobile ions are regarded as $n_i = n_o$ and $n_e = n_o \cdot \exp(\Phi/kT_e)$ from the Boltzmann relation for electrons. Thus, λ_D is known to be

$$\lambda_D = \sqrt{\frac{\varepsilon_0 \cdot kT_e}{e \cdot n_e}} \cong 743 \cdot \sqrt{\frac{T_e(V)}{n_e(cm^{-3})}} \ [cm] \tag{2.2}$$

4

where n_e is the electron density (cm^{-3}), kT_e is the electron temperature (eV), and e is the charge of an electron [4, 7]. The sheath region is naturally derived from the Debye length. Since electrons are repelled back into the bulk plasma by the negatively charged wall, a net positive space charge will be formed in the sheath region. The sheath region, lying between the negatively charged cathode and the bulk plasma, has a length of three to ten times λ_D in order to maintain charge continuity between electrodes [4]. This sheath region is essential to maintain a plasma.

CHAPTER 3

1-D PHOTONIC CRYSTALS

3.1. Distributed Bragg Reflector

At wavelengths within the photonic band gap as shown in Figure 2(a), the incident wave partially reflects off each layer of dielectric material. The reflected waves are in phase, reinforcing one another. "Total wave" amplitude continuously decreases when it passes through each dielectric layer due to constructive interference from reflected wave. Thus, the total wave cannot propagate through the spatially periodic structures. In contrast, at a wavelength not in the photonic band gap, the reflected waves are out of phase and attenuated due to destructive interference. Thus, as presented in Figure 2(b), the "total wave" can propagate through the periodical structure with only slight attenuation.
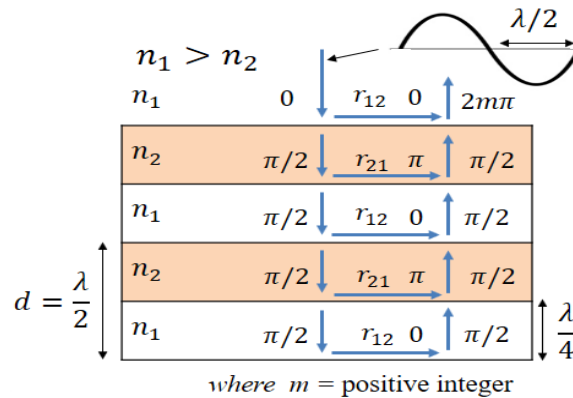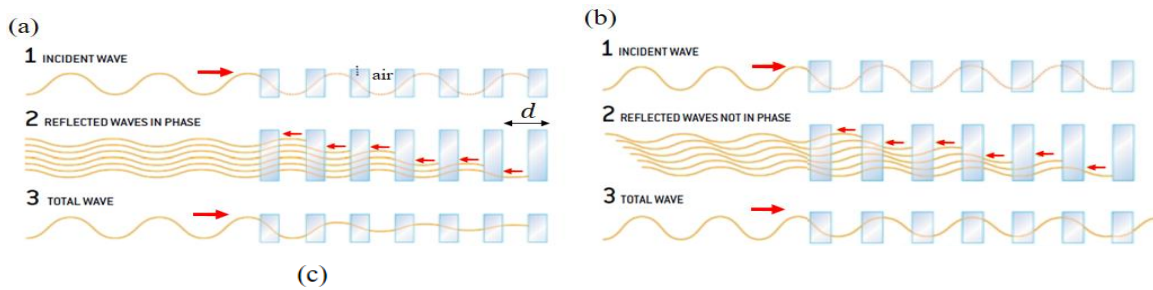

Figure 2. (a) Wavelength in the photonic bandgap: the constructive interference of reflected waves [8]. (b) Wavelength not in the photonic bandgap: reflected waves are attenuated by the destructive interference [8]. (c) Schematic representation of Distributed Bragg reflector.

As shown in Figure 2(c), a Bragg mirror, known as a distributed Bragg reflector, is a structure consisting of two different spatially periodic dielectric materials, and requires $d = \lambda/2$, where d is the lattice constant, and λ is the wavelength of the incident wave. Dielectric mirrors function based on the constructive interference of wave reflected from different layers. The structure has both high and low refractive indices, n_1 and n_2, respectively, and the reflection coefficient equation is $r_{12} = -r_{21} = \frac{n_1 - n_2}{n_1 + n_2}$. Specifically, the reflection from high to low refractive index at boundary, r_{12}, as shown in Figure 2(c), has a phase shift of zero due to internal reflection, in that r_{12} is positive when n_1 is greater than n_2. However, the reflection from low to high refractive index boundary, r_{21}, has a phase shift of π since there is an external reflection. Thus, the total phase shift for each reflected wave is an integer multiple of 2π, which result in constructive interference of reflected wave.

CHAPTER 4

REFRACTIVE INDEX FOR PLASMA PHOTONIC CRYSTALS

4.1. Refractive Index of Microplasma

It is well known that electric permittivity (ε) and magnetic permeability (μ) are fundamental characteristics determining the propagation of electromagnetic waves in matter. Calculating plasma refractive index as a function of the frequency of electromagnetic waves is important because an index contrast between two different spatially periodic dielectric materials is the main concept of plasma photonic crystals. The refractive index equation is the square root of the product of relative permittivity and relative permeability. The relative permeability can be assumed to be 1, since plasma is a non-magnetized material. The refractive index of plasma is $n = \sqrt{\varepsilon_r \mu_r} = \sqrt{\varepsilon_r}$ and can be written in complex form as shown in equation (4.1) [9, 10].

$$n_p(\omega) = \sqrt{\varepsilon_r(\omega)} = n_p' + i \cdot n_p'' \tag{4.1}$$

The complex form of the relative permittivity, $\varepsilon_r(\omega)$, can be derived using the Drude model [11]. Based on the Drude model expression, the dielectric constant of a plasma is dependent on the incident electromagnetic wave frequency, the plasma frequency and the collisional frequency, as shown in equation (4.2).

$$\varepsilon_r(\omega) = 1 - \frac{\omega_P^2}{\omega^2 \cdot \left(1 + i \cdot \frac{v_m}{\omega}\right)}$$

$$= \left(1 - \frac{\omega_P^2}{v_m^2 + \omega^2}\right) + i \cdot \frac{\omega_P^2 \cdot v_m}{(v_m^2 + \omega^2) \cdot \omega} \tag{4.2}$$

The parameter n_p' and n_p'' are the refractive index and the plasma's absorption for an electromagnetic wave, respectively.

4.2. Plasma Frequency and Collisional Frequency

The collisional frequency for momentum transfer, υ_m, represents the rate at which an electron collides with atoms. It is known to be approximately by

$$\upsilon_m \approx 10^9 \cdot p \text{ (Torr) [Hz]} \qquad (4.3)$$

where υ_m is clearly dependent on the neutral gas pressure and the cross section of elastic collision [2].

The plasma frequency, ω_p, is the frequency of electron oscillation around the ions, which can be derived from the Drude model [11] as

$$\omega_p = \sqrt{\frac{n_e \cdot e^2}{\varepsilon_o \cdot m_e}} = 5.634 \times 10^4 \cdot \sqrt{n_e \text{ (cm}^{-3})} \text{ [Hz]} \qquad (4.4)$$

where m_e is the mass of an electron and ε_o is the free space permittivity [4]. The plasma frequency can be described as the rapid oscillation of the electron density around the ions if a charge imbalance exists. When the displacement of the electrons to the right leaves an excess of ions on the left side of plasma and negative charge on the right side of plasma, the electric field points toward the right. The electric field pulls the electrons back toward their original locations and electrons move farther from their original positions due to gained kinetic energy from electron acceleration.
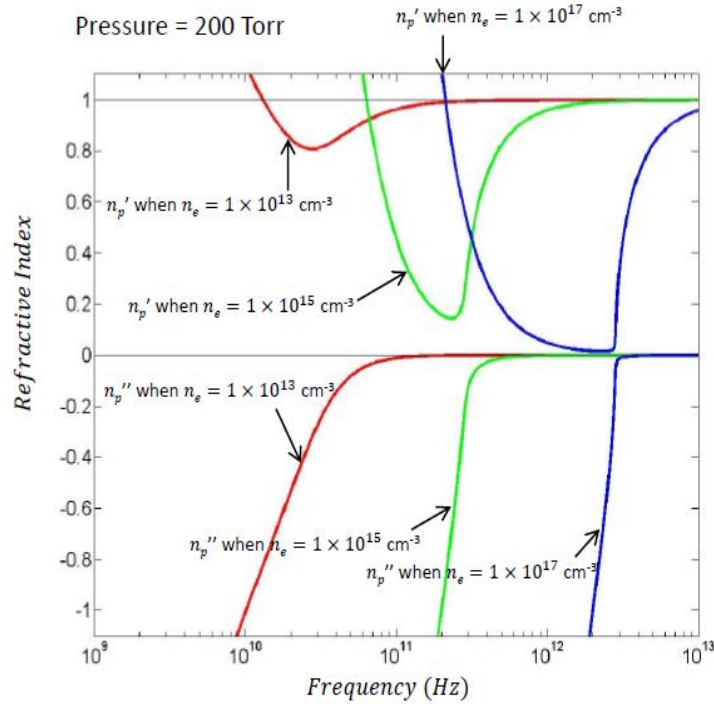
Figure 3. Refractive index depends on electron density and wavelength at 200 Torr gas pressure.

The refractive index of the plasma as a function of frequency at a pressure of 200 Torr is shown in Figure 3. The real part of refractive index n_p' in the upper half of Figure 3 is the usual refractive index, while the imaginary part of the refractive index n_p'' in the lower portion is the plasma's absorption of electromagnetic wave. The plasma's absorption coefficient for an electromagnetic wave at frequency ω is given by $\alpha(\omega) = 4\pi \cdot n_p''/\lambda$ where is calculated from the imaginary part of refractive index [11]. Photonic crystals can be optimized when the positive portion of refractive index is sufficiently different from that of air (n = 1) and an absorption coefficient from the negative portion is close to zero.

CHAPTER 5

PREVIOUS STUDY OF 2-D PLASMA PHOTONIC CRYSTALS

Figure 4(a) illustrates arrays of microplasma devices with lattice constant of 2.5 mm from Osamu Sakai of Kyoto University, Kyoto, Japan, who is one of the leading pioneers of plasma photonic crystals [9]. The photonic band gap exists around 60 GHz and can be calculated from the Bragg's law. A plot of the Bragg's law, $v_B = c/(2 \cdot a)$ as a function of lattice constant, a, is shown in Figure 5, where c is the speed of light [1]. Figure 5 illustrates the working frequency of photonic crystal device.

Figure 4. (a) Device with array of microplasma discharging with lattice constant of 2.5 mm. (b) Frequency dependence of transmittance signals as a function of applied voltage. (c) Frequency dependence of transmittance signals as a function of pressure [12].

Sakaguchi *et al.* tested the dependence of transmittance on applied voltage and pressure [12]. Low transmittance around the 60 GHz range in Figure 4(b) and (c) shows that the device with lattice constant 2.5 mm operates properly as photonic crystals. Low transmittance was measured

with increased voltage due to a higher electron density, which in turn decreased the real part of the relative permittivity in equation (4.2), as shown in Figure 4(b). This is because plasma frequency increases as electron density increases.
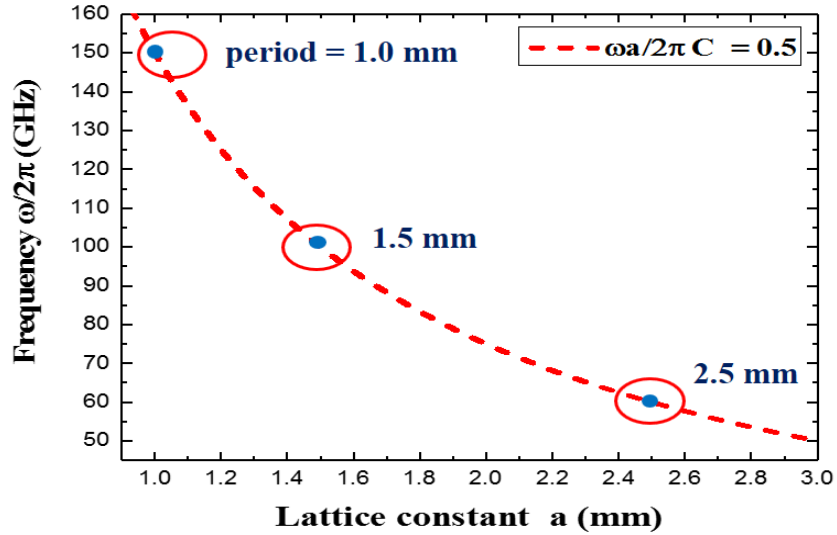
Figure 5. Bandgap frequency as a function of lattice constant (adapted from Ref. 12).

In addition, the transmittance drops became smaller as the pressure was increased as shown in Figure 4(c), since lower pressure corresponds to lower collision frequency according to equation (4.3). Thus, applying higher voltage and lower pressure decreases the real part of refractive index, providing higher index contrast between plasma and air with low transmittance [9, 12].

Figure 6(a) shows another device with lattice constant of 1.5 mm [12]. The Bragg's frequency of this device is at 100 GHz as shown in Figure 5. The transmittance in Figure 6(b) is around 85%, meaning this device does not operate properly as photonic crystals. As discussed, the main concept of plasma photonic crystals is spatially periodic variation of the refractive index between plasma and air. However, the boundaries between plasma columns and air is not well defined, impeding the periodicity of photonic crystals as shown in Figure 6(a). In addition, the real part of relative
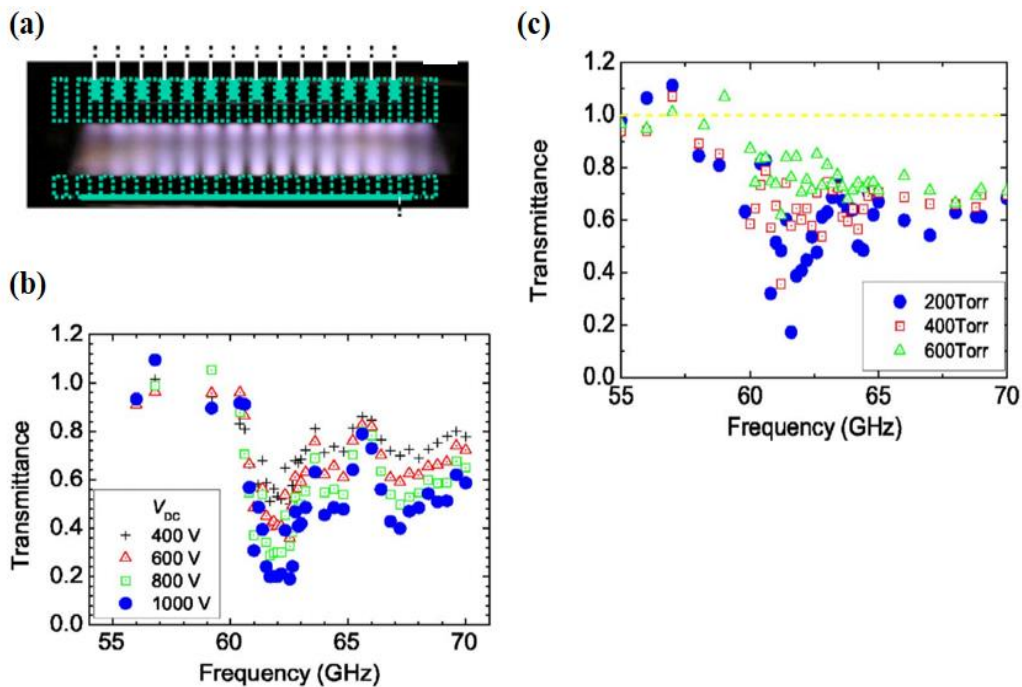
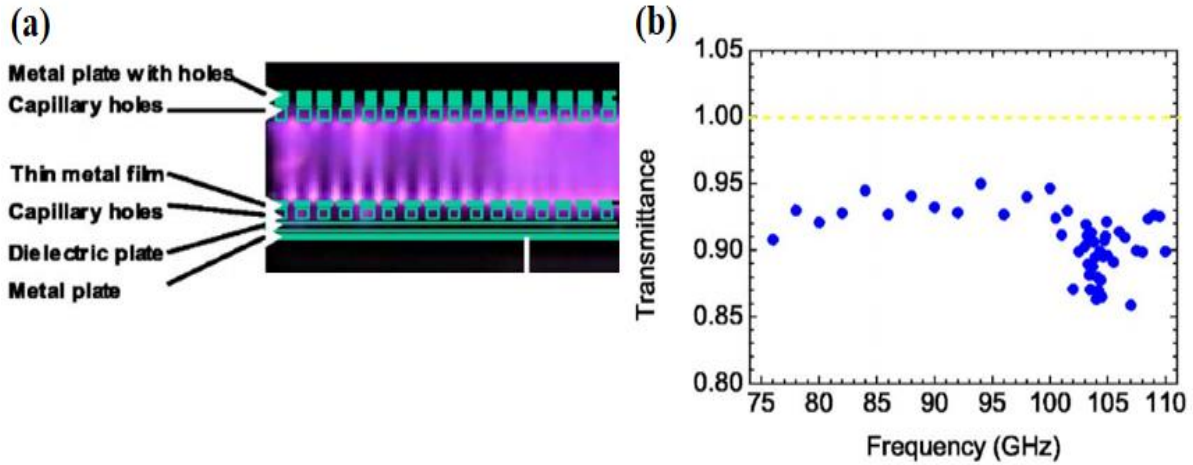Figure 6. (a) Device with array of microplasma discharging with lattice constant of 1.5 mm. (b) Frequency dependence of transmittance signals [12].

permittivity with 100 GHz is closed to 1 with electron density of 1×10^{13} cm^{-3}, which results in lower index contrast. Therefore, the device with higher electron density and well-defined boundaries is required to cover a working frequency of 100 GHz and beyond [9].

CHAPTER 6

2-D PLASMA PHOTONIC CRYSTALS

6.1. Device Fabrication

The device illustrated in Figures 7 and 8 is developed here at University of Illinois. It has higher electron densities and more defined boundaries compared to that of Figure 6(a). In this study, arrays of microplasma jets will be utilized to produce arrays of plasma columns for photonic crystals. As shown in Figure 7, the device suitable for use as 2-D plasma photonic crystals has been fabricated by room temperature vulcanization (RTV) of silicon and copper wires. Helium gas will flow through the array of microchannels embedded in the RTV silicon and 2.5 kV$_{pk-pk}$ with 20 kHz sinusoidal driving waveform will be used to operate this device. The length of the plasma jet from Figure 8(b) is approximately 1 mm, which is not sufficient for photonic crystals; however, as illustrated in Figure 8(c), it can be extended up to 5 mm by placing extra metal rods near the edge of plasma jets. We expect this device to cover around 150 GHz Bragg's frequency, as illustrated in Figure 5.

A set of three electrodes will determine the position of plasma jets, allowing the activation/deactivation of each plasma array. Since array subsets of plasma jets can be turned on and off at will, the arrays will work as reconfigurable plasma photonic crystals at electronic speeds which, in turn, will allow for the transmittance characteristic to be altered rapidly.
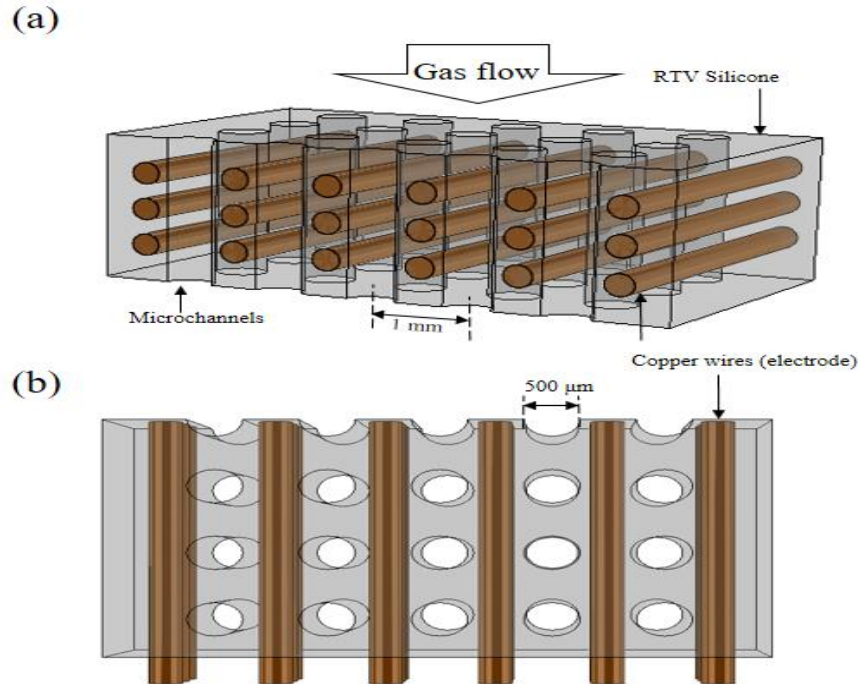
Figure 7. (a) Cross-sectional diagram, (b) top view for 2-D plasma photonic crystals device.
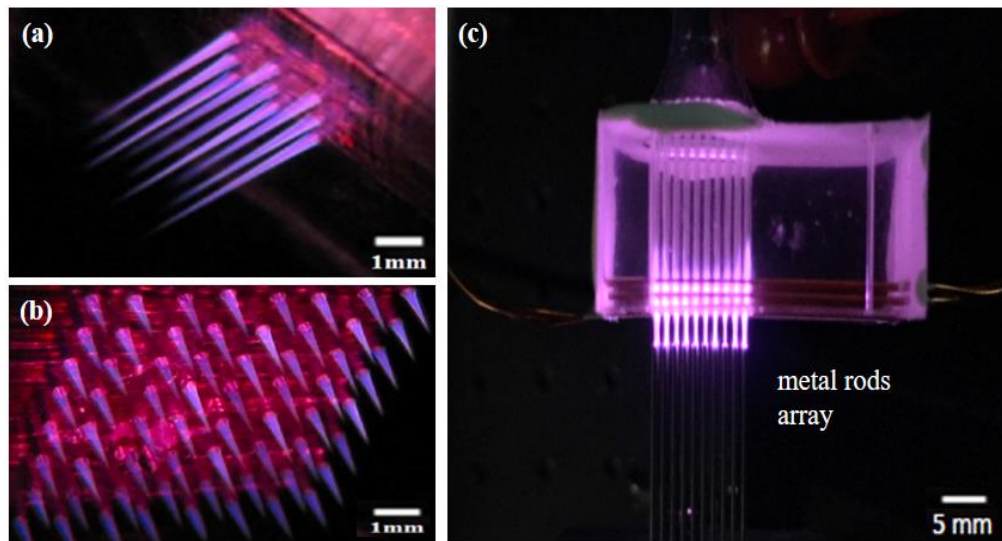

Figure 8. (a) Perspective view of array of microplasma jets (3 x 3) [13]. (b) Perspective view of array of microplasma jets (10 x 10). (c) Side view of 2-D plasma photonic crystals device with extended array of microplasma jets by placing external metal rods array.

6.2. Experimental Arrangement

The experiment setup for 2-D plasma photonic crystals is illustrated in Figure 9. Signal generator (E8257D-520, Keysight Technologies) is utilized to generate microwave in a range of 9 to 15 GHz. In order to verify the working frequency of arrays of microplasma (~150 GHz), microwave from signal generator should be multiplied by 12 times through a signal generator extension module (WR6.5 AMC, Virginia Diodes Inc.). Amplified microwave passing through arrays of microplasma needs to be decreased by tunable synthesizer and frequency mixer (WR6.5 MixAMC, Virginia Diodes Inc.) by a factor of 12 in order to satisfy the detectable range of spectrum analyzer (PXA Signal Analyzer N9030A, Keysight Technologies).

```
┌──────────────────┐      ┌──────────────────┐      ┌──────────────────┐
│   Horn Antenna   │─────▶│ Microplasma Array│─────▶│   Horn Antenna   │
│                  │      │     (10 x 5)     │      │                  │
└──────────────────┘      └──────────────────┘      └──────────────────┘
        ▲                                                     │
   (110 – 170 GHz)                                      (110 – 170 GHz)
        │                                                     ▼
┌──────────────────┐      ┌──────────────────┐      ┌──────────────────┐
│    Frequency     │      │     Tunable      │      │    Frequency     │
│ Multiplier (N=12)│      │   Synthesizer    │─────▶│  Mixer (N = 12)  │
└──────────────────┘      └──────────────────┘ f₂   └──────────────────┘
        ▲                                                     │
   f₁  (9 – 15 GHz)              (9 – 15 GHz)              f_out
        │                                                     ▼
┌──────────────────┐                              ┌──────────────────┐
│ Signal Generator │        f_out = N(f₁ – f₂)    │ Spectrum Analyzer│
│  (DC – 20 GHz)   │                              │  (DC – 26.5 GHz) │
└──────────────────┘                              └──────────────────┘
```
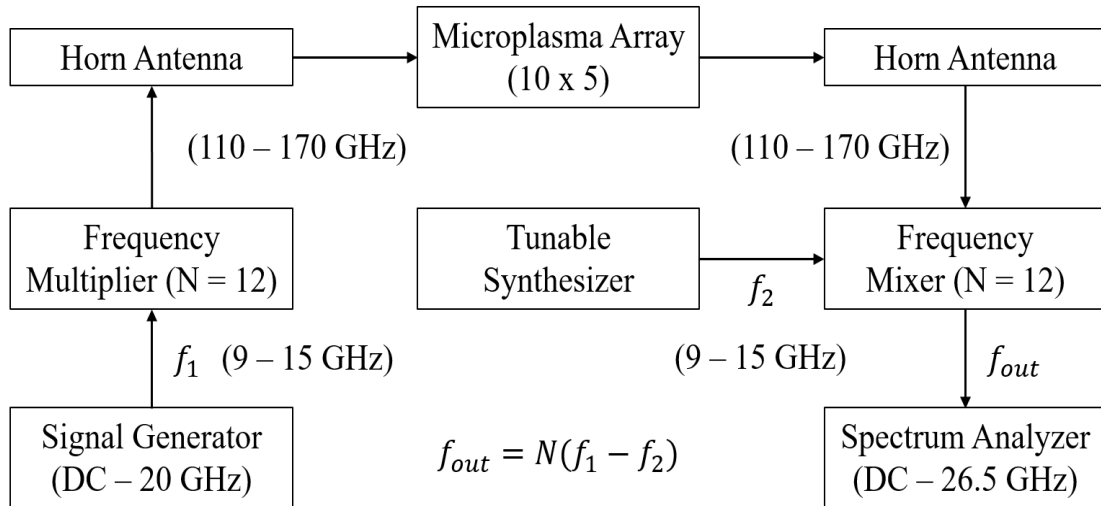
$$f_{out} = N(f_1 - f_2)$$

Figure 9. Experimental arrangement for 2-D plasma photonic crystals.

6.3. Data Collection

Figure 10 illustrated the experimental result of 2-D plasma photonic crystals that is the measurement of the normalized transmission of 5×10 arrays, in 0.1 GHz increments over the 150 – 160 GHz. As expected, 2-D plasma photonic crystal device can cover around 150 GHz Bragg's frequency, as illustrated in Figure 5. The time-averaged attenuation at 157 GHz is 5 % and it can
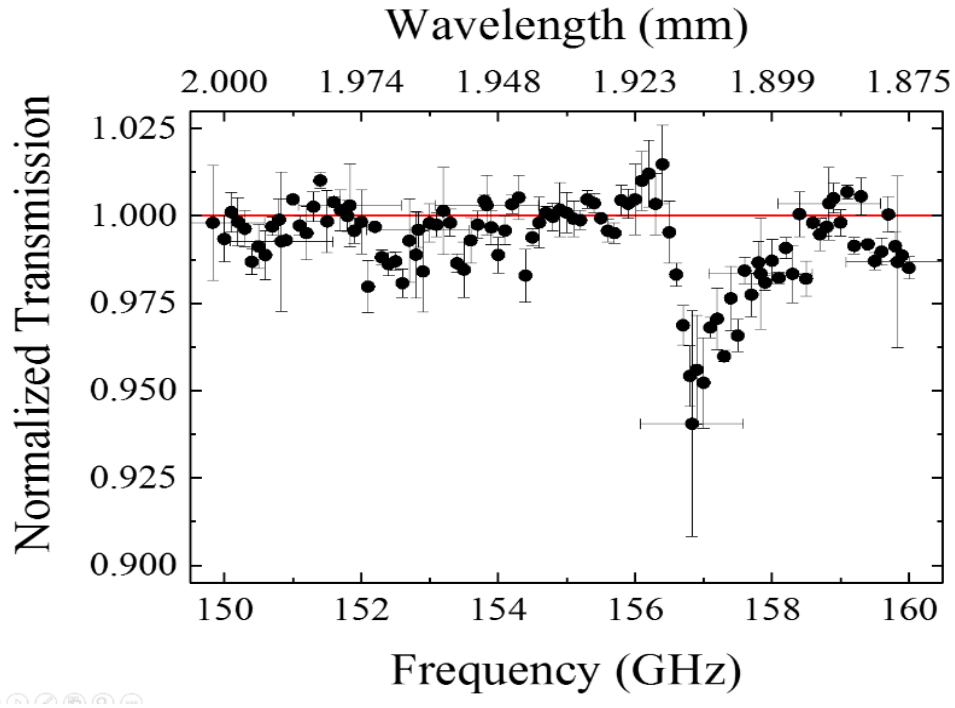
Figure 10. Experimental result of 2-D plasma photonic crystals [14].

be increased by adjusting electron density, gas pressure and quantity of arrays of microplasma jets. In addition, the applied source to generate arrays of microplasma is alternative voltage (AC) for which the duty cycle is less than 20 %. Compared with other plasma sources such as DC and pulse sources, this result indicates a fairly good attenuation at 157 GHz since plasma is activated in a few microseconds in a cycle [14].

CHAPTER 7

CONCLUSIONS AND FUTURE STUDY

Photonic crystals composed of microplasma arrays will be further studied. The working frequency derived from the Bragg's frequency and the contrast of refractive index between two different spatially periodic material, plasma and air, determine the transmittance of electromagnetic waves. In addition, by varying the lattice constant of the device, the range working frequency (Bragg's law) is able to be controlled. In comparison to Sakai's research, a much wider range of the electromagnetic spectrum will be accessible to our plasma photonic crystal device due to its well-defined boundaries and higher electron density. This photonic crystal device will be tested at lower pressure (~200 Torr) with helium gas to confirm that it can serve as photonic crystals. Furthermore, photonic crystals comprising arrays of microplasma will be fabricated to cover the THz spectral region.

REFERENCES

[1] B. E. A. Saleh and M. C. Teich, *Fundamentals of Photonics*. Wiley & Sons, 2007.

[2] A. Fridman and L. A. Kennedy, *Plasma Physics and Engineering*. New York, NY: CRC Press, 2004.

[3] Y. P. Raizer, *Gas Discharge Physics*. Springer, 1991.

[4] M. A. Lieberman, and A. J. Lichtenberg, *Principle of Plasma Discharges and Material Processing*. Wiley-Interscience, 2005.

[5] M. H. Kim, J. H. Cho, S. B. Ban, R. Y. Choi, E. J. Kwon, S.-J. Park, and J. G. Eden, "Efficient generation of ozone in arrays of microchannel plasmas," *J. Phys. D. Appl. Phys.*, vol. 46, p. 305201, 2013.

[6] K. H. Becker, K. H. Schoenbach, and J. G. Eden, "Microplasmas and applications," *J. Phys. D: Appl. Phys.*, 39, R55–R70, 2006.

[7] B. E. Cherrington, *Gaseous Electronics and Gas Lasers*. Pergamon Press, 1979.

[8] E. Yablonovitch, "Photonic crystals: Semiconductors of light," *Scientific American*, 47-55, Dec. 2001.

[9] O. Sakai, T. Sakaguchi, Y. Ito, and K. Tachibana, "Interaction and control of millimetre-waves with microplasma arrays," *Plasma Phys. Control. Fusion*, vol. 47, no. 12B, pp. B617–B627, Dec. 2005.

[10] O. Sakai and K. Tachibana, "Properties of electromagnetic wave propagation emerging in 2-D periodic plasma structures," *IEEE Trans. Plasma Sci.*, vol. 35, no. 5, pp. 1267–1273, 2007.

[11] S. L. Chuang, *Physics of Photonic Devices*. Wiley & Sons, 2009.

[12] T. Sakaguchi, O. Sakai, and K. Tachibana, "Photonic bands in two-dimensional microplasma arrays. II. Band gaps observed in millimeter and subterahertz ranges," *J. Appl. Phys.*, vol. 101, no. 7, p. 073305, 2007.

[13] P. P. Sun, J. H. Cho, C. H. Park, S. J. Park, and J. G. Eden, "Close-packed arrays of plasma jets emanating from microchannels in a transparent polymer," *IEEE Trans. Plasma Sci.*, vol. 40, no. 11, pp. 2946–2950, 201.

[14] H. J. Yang, S. -J. Park, and J. G. Eden (to be published).